Research Article | Vol. 26, No. 1 | 8 Jan 2018 | OPTICS EXPRESS 32
Optics EXPRESS

Experimental observation of quantum state-independent contextuality under no-signaling conditions

YA XIAO,[1,2,3] ZHEN-PENG XU,[3,4] QIANG LI,[1,2] JIN-SHI XU,[1,2,5] KAI SUN,[1,2] JIN-MING CUI,[1,2] ZONG-QUAN ZHOU,[1,2] HONG-YI SU,[4,6] ADÁN CABELLO,[7] JING-LING CHEN,[4,8,9] CHUAN-FENG LI,[1,2,10] AND GUANG-CAN GUO[1,2]

[1]*CAS Key Laboratory of Quantum Information, University of Science and Technology of China, Hefei 230026, China*
[2]*Synergetic Innovation Center of Quantum Information and Quantum Physics, University of Science and Technology of China, Hefei 230026, China*
[4]*Theoretical Physics Division, Chern Institute of Mathematics, Nankai University, Tianjin 30071, China*
[6]*Department of Physics Education, Chonnam National University, Gwangju 500-757, South Korea*
[7]*Departamento de Física Aplicada II, Universidad de Sevilla, E-41012 Sevilla, Spain*
[8]*Centre for Quantum Technologies, National University of Singapore, 3 Science Drive 2, Singapore 117543, Singapore*
[3]*These two authors contributed equally to this work.*
[5]*jsxu@ustc.edu.cn*
[9]*chenjl@nankai.edu.cn*
[10]*cfli@ustc.edu.cn*

Abstract: Contextuality, the impossibility of assigning context-independent measurement outcomes, is a critical resource for quantum computation and communication. No-signaling between successive measurements is an essential requirement that should be accomplished in any test of quantum contextuality and that is difficult to achieve in practice. Here, we introduce an optimal quantum state-independent contextuality inequality in which the deviation from the classical bound is maximal. We then experimentally test it using single photons generated from a defect in a bulk silicon carbide, while satisfying the requirement of no-signaling within the experimental error. Our results shed new light on the study of quantum contextuality under no-signaling conditions.

OCIS codes: (270.0270) Quantum optics; (270.5585) Quantum information and processing; (000.2190) Experimental physics.

References and links

1. E. P. Specker, "Die Logik nicht gleichzeitig entscheidbarer Aussagen," Dialectica **14**, 239–246 (1960).
2. M. P. Seevinck, " E. Specker: 'The logic of non-simultaneously decidable propositions' (1960)," arXiv: 1103.4537 (2011).
3. J. B. Bell, "On the Problem of Hidden Variables in Quantum Mechanics," Rev. Mod. Phys. **38**, 447 (1966).
4. S. Kochen, and E. P. Specker, "The problem of hidden variables in quantum mechanics," J. Math. Mech. **17**, 59–87 (1967).
5. A. Cabello, "Simple Explanation of the Quantum Violation of a Fundamental Inequality," Phys. Rev. Lett. **110**, 060402 (2013).
6. B. Yan, "Quantum Correlations are Tightly Bound by the Exclusivity Principle," Phys. Rev. Lett. **110**, 260406 (2013).
7. G. Chiribella, and X. Yuan, "Measurement sharpness cuts nonlocality and contextuality in every physical theory," arXiv: 1404.3348 (2014).
8. A. Cabello, "Simple Explanation of the Quantum Limits of Genuine *n*-Body Nonlocality," Phys. Rev. Lett. **114**, 220402 (2015).
9. M. Howard, J. Wallman, V. Veitch, and J. Emerson, "Contextuality supplies the "magic" for quantum computation," Nature **510**, 351–355 (2014).

#306961 https://doi.org/10.1364/OE.26.000032
Journal © 2018 Received 13 Sep 2017; revised 8 Dec 2017; accepted 9 Dec 2017; published 2 Jan 2018

Optics EXPRESS

10. R. Raussendorf, "Contextuality in measurement-based quantum computation," Phys. Rev. A **88**, 022322 (2013).
11. K. Horodecki, M. Horodecki, P. Horodecki, R. Horodecki, M. Pawlowski, and M. Bourennane, "Contextuality offers device-independent security," arXiv: 1006.0468 (2010).
12. S. Yu, and C. H. Oh, "State-Independent Proof of Kochen-Specker Theorem with 13 Rays," Phys. Rev. Lett. **108**, 030402 (2012).
13. M. Kernaghan, "Bell-Kochen-Specker theorem for 20 vectors," J. Phys. A: Math. Gen. **27**, L829–L830 (1994).
14. A. Cabello, J. M. Estebaranz, and G. García-Alcain, "Bell-Kochen-Specker theorem: A proof with 18 vectors," Phys. Lett. A **212**, 183–187 (1996).
15. M. Kernaghan, and A. Peres, "Kochen-Specker theorem for eight-dimensional space," Phys. Lett. A **198**, 1–5 (1995).
16. A. Cabello, M. Kleinmann, and C. Budroni, "Necessary and Sufficient Condition for Quantum State-Independent Contextuality," Phys. Rev. Lett. **114**, 250402 (2015).
17. A. Cabello, M. Kleinmann, and J. R. Portillo, "Quantum State-Independent Contextuality Requires 13 Rays," J. Phys. A: Math. Theor. **49**, 38LT01 (2016).
18. N. Brunner, D. Cavalcanti, S. Pironio, V. Scarani, and S. Wehner, "Bell nonlocality," Rev. Mod. Phys. **86**, 419–478 (2014).
19. C. Zu, Y.-X. Wang, D.-L. Deng, X.-Y. Chang, K. Liu, P.-Y. Hou, H.-X. Yang, and L.-M. Duan, "State-Independent Experimental Test of Quantum Contextuality in An Indivisible System," Phys. Rev. Lett. **109**, 150401 (2012).
20. Y.-F. Huang, M. Li, D.-Y. Cao, C. Zhang, Y.-S. Zhang, B.-H. Liu, C.-F. Li, and G.-C. Guo, "Experimental test of state-independent quantum contextuality of an indivisible quantum system," Phys. Rev. A **87**, 052133 (2013).
21. X. Zhang, M. Um, J. Zhang, S. An, Y. Wang, D.-L. Deng, C. Shen, L.-M. Duan, and K. Kim, "State-Independent Experimental Test of Quantum Contextuality with a Single Trapped Ion," Phys. Rev. Lett. **110**, 070401 (2013).
22. G. Kirchmair, F. Zähringer, R. Gerritsma, M. Kleinmann, O. Gühne, A. Cabello, R. Blatt, and C. F. Roos, "State-independent experimental test of quantum contextuality," Nature **460**, 494–497 (2009).
23. A. Cabello, "Simple method for experimentally testing any form of quantum contextuality," Phys. Rev. A **93**, 032102 (2016).
24. A. Cabello, S. Severini, and A. Winter, "Graph-Theoretic Approach to Quantum Correlations," Phys. Rev. Lett. **112**, 040401 (2014).
25. S. Castelletto, B. C. Johnson, V. Ivády, N. Stavrias, T. Umeda, A. Gali, and T. Ohshima, "A silicon carbide room-temperature single-photon source," Nature Mat. **13**, 151–156 (2014).
26. M. Kleinmann, C. Budroni, J.-Å. Larsson, O. Gühne, and A. Cabello, "Optimal Inequalities for State-Independent Contextuality," Phys. Rev. Lett. **109**, 250402 (2012).
27. R. Ramanathan, and P. Horodecki, "Necessary and sufficient condition for state-independent contextual measurement scenarios," Phys. Rev. Lett. **112**, 040404 (2014).
28. C. Monroe, and J. Kim, "Scaling the ion trap quantum processor," Science **339**, 1164–1169 (2013).
29. A. Cabello, M. Gu, O. Gühne, J. Larsson, and K. Wiesner, "Thermodynamical cost of some interpretations of quantum theory," Phys. Rev. A **94**, 052127 (2016).
30. A. Tavakoli, and A. Cabello, "Cost of classically simulating quantum sequential measurements on entangled systems," arXiv:1705.07456 (2017).
31. A. Cabello, M. Gu, O. Gühne, and Z.-P. Xu, "Optimal simulation of state-independent quantum contextuality," arXiv:1709.07372 (2017).

1. Introduction

Quantum mechanics has many features that are inconsistent with classical models. One of them is quantum contextuality [1–4], i.e., the impossibility of assigning context-independent measurement outcomes in agreement with the quantum predictions. On the other hand, according to noncontextual hidden-variable models, its value is completely independent of all the other observables that the experimenter may decide to measure at the same time. Quantum contextuality has been shown to play important roles in fundamental quantum physics [5–8] and practical quantum information processing [9–11].

Furthermore, contextuality offers an unusual perspective on the striking features of the quantum world by pointing out scenarios in which primitive notions such as preparations and states play no role. This is known as state-independent contextuality (SIC) [12–15]. It has been recently proven [16, 17] that the simplest of these scenarios is the one introduced by Yu and Oh [12], consisting in a set of 13 elementary measurements on a three-dimensional quantum system (or qutrit). By simplest scenario we mean the one requiring a minimal number of elementary measurements (i.e., sharp measurements [7] having only two outcomes, one of them nondegenerate). For practical purposes, given set of measurements revealing SIC, it is helpful to identify which is the optimal quantum state-independent violation of the non-contextuality

Optics EXPRESS

inequalities (NCIs) that use this set. Optimality is defined as the case in which the ratio between the prediction of quantum mechanics and the classical bound is maximal. A larger deviation from the classical bound implies in this case more robustness against experimental imperfections.

In any contextuality experiment with sequential measurements there is a crucial assumption, namely, that there should be no signaling between one measurement and the next (the same way in a Bell inequality experiment [18], the crucial assumption is that there is no signaling between Alice and Bob). If this no-signaling condition cannot be satisfied, then experimental probabilities are contextual and thus it is unreasonable and quite arbitrary to assume that measurement outcomes must be non-contextual. In other words, unless one observes no signaling between the successive measurements, the bound of the non-contextuality inequality has no physical motivation whatsoever. Previous experiments attempted to observe the simplest form of SIC in the Yu-Oh scenario did not show to satisfy such condition [19–21]. The experiment in [22] satisfies no-signaling within the experimental error. However, it is not a test of SIC with qutrits but with pairs of qubits.

The aim of this work is to experimentally observe the quantum violation of optimal SIC inequality for the Yu-Oh scenario under the no-signaling condition. That is, guaranteeing that the marginal probabilities of all the measurement outcomes are the same in any context during the test. We first define a parameter to identify the optimal 13-ray SIC in the Yu-Oh scenario. To obtain the no-signaling condition, we use a recent method proposed for performing contextuality experiments on systems in which non-demolition measurements are difficult [23] and apply it to single photons generated from a defect in a bulk silicon carbide. This allows us to achieve a very high control of the measurement and assure that, within the experimental error, there is no-signaling. In our case, the no-signaling is defined as if $\forall A$, $P(a|A) = \sum_b P(a, b|A, B)$, $\forall B$; and $\forall B$, $P(b|B) = \sum_a P(a, b|A, B)$, $\forall A$. A and B are sequential measurements with the results of a and b, respectively. Due to the statistical property of no-signaling condition, there is still probability (within experimental error bars) to communicate between the two sequential measurements. Our results agree with the quantum mechanical predictions that are inconsistent with noncontextual hidden variable models. These results will be helpful for future tests and applications of quantum contextuality.

2. Theoretical framework

Graphs have been shown to be useful in investigating quantum correlations. A powerful graph-theoretic approach to investigate contextuality was proposed by Cabello, Severini, and Winter (CSW) [24]. There, measurement events, defined as state transformations due to sharp measurements, are represented as vertices of a graph, and exclusive events, defined as those corresponding to different outcomes of a sharp measurement, are represented by vertices connected by an edge. This way, the events in every NCI can be represented by a graph called the exclusivity graph. Interestingly, many characteristic numbers of this graph correspond to important physical bounds. In particular, the independence number of the graph, denoted as $\alpha(G)$, gives the non-contextual bound and the Lovász number of the graph, denoted as $\vartheta(G)$ gives the quantum maximum.

On the other hand, given N distinct rays $|v_i\rangle$, representing possible final quantum states after an ideal measurement of the observable represented by $\hat{P}_i = |v_i\rangle\langle v_i|$, one can consider the following quantity:

$$I = \sum_{i=1}^{N} w_i \langle \hat{P}_i \rangle \leq \alpha(G), \tag{1}$$

where $w_i > 0$ are weights and $\langle \hat{P}_i \rangle$ denote average values. $\alpha(G)$ is the independence number of the weighted graph G in which vertices correspond to rays, edges connect orthogonal rays,

Optics EXPRESS

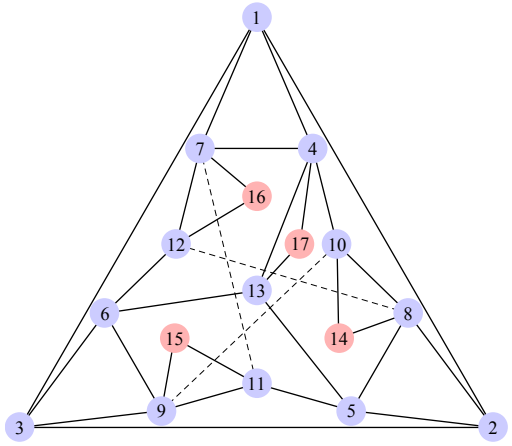

Fig. 1. Graph of the exclusivity relations between the measurements for the Yu-Oh scenario. Vertices represent vectors v_i and edges represent exclusivity relations. The blue vertices represent the vectors in the Yu-Oh set. The red vertices represent the extra vectors used for assuring that each projector is always measured using a complete basis. The states are represented as $v_1 = (1,0,0)$, $v_2 = (0,1,0)$, $v_3 = (0,0,1)$, $v_4 = \frac{1}{\sqrt{2}}(0,1,-1)$, $v_5 = \frac{1}{\sqrt{2}}(1,0,-1)$, $v_6 = \frac{1}{\sqrt{2}}(1,-1,0)$, $v_7 = \frac{1}{\sqrt{2}}(0,1,1)$, $v_8 = \frac{1}{\sqrt{2}}(1,0,1)$, $v_9 = \frac{1}{\sqrt{2}}(1,1,0)$, $v_{10} = \frac{1}{\sqrt{3}}(-1,1,1)$, $v_{11} = \frac{1}{\sqrt{3}}(1,-1,1)$, $v_{12} = \frac{1}{\sqrt{3}}(1,1,-1)$, $v_{13} = -\frac{1}{\sqrt{3}}(1,1,1)$, $v_{14} = \frac{1}{\sqrt{6}}(1,2,-1)$, $v_{15} = \frac{1}{\sqrt{6}}(1,-1,-2)$, $v_{16} = \frac{1}{\sqrt{6}}(2,-1,1)$, $v_{17} = \frac{1}{\sqrt{6}}(2,-1,-1)$, respectively.

and the vertex weights are the w_i. Inequality (1) is not yet a NCI as $\alpha(G)$ is the noncontextual bound only under the assumption that orthogonal rays correspond to exclusive events obtained by sequentially measuring compatible ideal measurements each of them appearing in different contexts. However, the method in [23] allows us to, given any interesting set of rays, produce a proper NCI that can be tested with sequential measurements. In addition, if the set of rays is a SIC set and the choice of weights is appropriate, then the resulting NCI is such that its quantum violation I_{QM} is a constant, that is, the NCI is violated equally by all quantum states.

In this work our quantum system is a qutrit. We use the basis $\{|i_1\rangle, |i_2\rangle, |i_3\rangle\}$ to express its states, and focus on observing quantum SIC for the Yu-Oh set. The Yu-Oh elementary measurements correspond to the projectors onto the vectors $|v_i\rangle$ in Fig. 1 and are represented there by blue vertices numerated from 1 to 13. In our work, the optimal inequality adopted to demonstrate SIC is given by

$$I = 3\sum_{i=1}^{9}\langle\hat{P}_i\rangle + 2\sum_{i=13}^{10}\langle\hat{P}_i\rangle \leq 11, \tag{2}$$

with $I_{\mathrm{QM}} = 35/3$ for all quantum states. By the optimal SIC inequality we mean the one for which the ratio $I_{\mathrm{QM}}/\alpha(G)$ is maximal over all possible weights w_i (see Appendix A for more details).

To demonstrate the quantum SIC under no-signaling conditions, we resort to the method in [23] which has the virtue of preserving the ratio $I_{\mathrm{QM}}/\alpha(G)$. In an ideal contextuality test, the probabilities of the outcomes of each subsequent measurement should not be affected by any previous measurement. However, experiment errors make that this condition approximately satisfied. Following the suggestion in [23], here we assume that the no-signaling condition can be

Optics EXPRESS

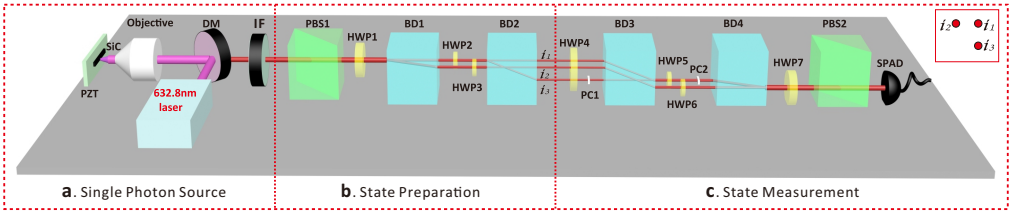

Fig. 2. Experimental setup to test the noncontextuality inequality. **(a).** The preparation of a single photon source. A single photon is generated by using a 632.8 nm laser to excite an intrinsic defect in a 4H-SiC sample which is mounted on a piezoelectric XYZ stage (PZT). The dichroic mirror (DM) is used to separated the pump laser and the fluorescence, which is further filtered by an interference filter (IF) centered at 720 nm with a bandwidth of 13 nm. **(b).** State preparation of a single photon qutrit. The polarization of the photon is set to be horizontal by the polarization beam splitter 1 (PBS1). After passing the first three haft-wave plates (HWP1, HWP2 and HWP3) and two beam displacers (BD1 and BD2), the photon is split into three paths. By adjusting the angle settings of HWPs, we can prepare different initial qutrit states. **(c).** The setup for state measurement. The angle of HWP4 is set to 45° and the photon in paths 1 and 3 are combined by the BD3. Different measurement bases are implemented by rotating HWP5, HWP6, and HWP7. Several phase plates (PCs) are inserted into paths to compensate relative phases. The photon is then detected by a single-photon avalanche detector (SPAD).

reasonably assumed to be satisfied when the influence of past measurement on future measurements is indistinguishable from the influence of future measurements on past measurements, within the experimental precision. The detailed definitions of the influences are given in Appendix B.2. To compute the probabilities required in the method, we have to consider four additional projectors, $\{|v_{14}\rangle, |v_{15}\rangle, |v_{16}\rangle$, and $|v_{17}\rangle\}$, to make sure that every projector is measured as part of a complete basis. These extra projectors are represented in Fig. 1 by red vertices numerated from 14 to 17.

The NCI inequality resulting contains two-point correlations $P_{|\varphi\rangle}(v_i = 1, v_j = 1)$ $(= P_{|\varphi\rangle}(v_i = 1)P_{|v_i\rangle}(v_j = 1))$, that represent the experimental imprecision when $|v_i\rangle$ and $|v_j\rangle$ are measured successively. Applying this method, Eq. (2) is converted into the following inequality (3), which is the one tested in our experiment,

$$\begin{aligned} I^{\text{opt}} &= 3\sum_{i=1}^{9} P_{|\varphi\rangle}(v_i = 1)\left(1 - \frac{1}{2}\sum_{(i,j)\in E} P_{|v_i\rangle}(v_j = 1)\right) \\ &\quad + 2\sum_{i=10}^{13} P_{|\varphi\rangle}(v_i = 1)\left(1 - \frac{1}{2}\sum_{(i,j)\in E} P_{|v_i\rangle}(v_j = 1)\right) \\ &\leq 11, \end{aligned} \tag{3}$$

where $P_{|\varphi\rangle}(v_i = 1) = \langle\varphi|\hat{P}_i|\varphi\rangle$ $(P_{|v_i\rangle}(v_j = 1) = \langle v_i|\hat{P}_j|v_i\rangle)$ represents the probability to obtain v_i (v_j) when the input state is $|\varphi\rangle$ (v_i). The edge set E with $(i, j) \in E$ indicates that $|v_i\rangle$ and $|v_j\rangle$ are orthogonal, i.e., $\langle v_i|v_j\rangle = 0$. All non-contextual hidden variable models satisfy inequality (3), while the quantum theory predicts that, for any qutrit state, $I^{\text{opt}}_{\text{QM}} = 35/3$, which is shown to be optimal (see Appendix A for more details). Obviously, the quantum prediction is greater than the upper bound for non-contextual models. Therefore, inequality (3) can be used to test quantum SIC of a qutrit.

Optics EXPRESS

3. Experimental setup and results

Figure 2 shows our experimental setup. We prepared a single photon by exciting an intrinsic defect, known as the carbon antisite-vacancy pair in a bulk silicon carbide (SiC) sample [25], with a 632.8 nm laser, as shown in Fig. 2(a). After a bandpass filter with a central wavelength of 720 nm and a bandwidth of 13 nm to filter the fluorescence, the photon is first sent to a Hanbury Brown-Twiss interferometer to verify the character of the single-photon source (not shown in Fig. 2). The autocorrelation of the emission is typically measured to be $g^2(0) = 0.179$ with the fitting to 0.026, which demonstrates that it is a good-quality single-photon source (see Appendix B.1 for more details).

We then sent the photon into the contextuality test setup. Making use of half-wave plates (HWPs), which manipulate the polarization of the photons, and beam displacers (BDs), which separate polarized photons into different paths, we can prepare arbitrary pure states of a qutrit encoded in the path degrees of freedom of the input photon. This is shown in Fig. 2(b). The first polarization beam splitter (PBS1) is used to initialize the polarization of the photon to be horizontal. The amplitudes of the basis in the qutrit states can be changed by rotating HWP1, HWP2, and HWP3 conveniently. To prepare several diagonal mixed states, two birefringent crystals with different lengths are inserted after HWP1 and HWP2 (not shown in Fig. 2). Each birefringent crystal introduces a large enough time delay between $|H\rangle$ and $|V\rangle$ components. When the photon passes through them, the coherence among $|i_1\rangle$, $|i_2\rangle$ and $|i_3\rangle$ components is completely destroyed and the mixed state is produced.

The measurement setup is shown in Fig. 2(c). There, the quantum information encoded in spatial modes is converted back into polarization-encoded quantum information. The angle of HWP4 is set to be 45° and the paths i_1 and i_3 are combined to one path after BD3. HWP5 and HWP6 further change the polarizations in the corresponding paths and led them combined to only one path after BD4. HWP7 is set to rotate the polarization of the photon to be horizontal, which is selected by PBS2. The photon is finally detected by a single-photon avalanche detector (SPAD).

Since our detector has imperfect detection efficiency and our setup only measures rank-one projectors, to compute probabilities like $P_{|\varphi\rangle}(v_i = 1)$ when the input state is $|\varphi\rangle$, we need to measure v_i as part of a complete basis set of $\{v_i, v_{i'}, v_{i''}\}$. In a contextuality experiment, it is crucial to measure each observable v_i the same way with independence of the context. Thus, for each v_i, we always use the same orthogonal basis, and $P_{|\varphi\rangle}(v_i = 1)$ can be expressed as follows:

$$P_{|\varphi\rangle}(v_i = 1) = \frac{N_{|\varphi\rangle}(v_i)}{N_{|\varphi\rangle}(v_i) + N_{|\varphi\rangle}(v_{i'}) + N_{|\varphi\rangle}(v_{i''})}, \tag{4}$$

where $N_{|\varphi\rangle}(v_i)$ is the number of counts corresponding to outcome $(v_i = 1)$ when the system is prepared in state $|\varphi\rangle$ and we take a projective measurement of $|v_i\rangle$. In our case, there are seven group bases: $\{v_1, v_4, v_7\}$, $\{v_2, v_5, v_8\}$, $\{v_3, v_6, v_9\}$, $\{v_4, v_{13}, v_{17}\}$, $\{v_7, v_{12}, v_{16}\}$, $\{v_8, v_{10}, v_{14}\}$, and $\{v_9, v_{11}, v_{15}\}$. The methods to calculate the two-point probabilities can be found in Appendix B.2.

As emphasized before, in any test of contextuality, we should achieve no-signaling between the measurements in the same context. This implies that the influence between first measurements and second measurements (denoted as $\varepsilon(\_, 0|\_, v_j)$ and $\varepsilon(\_, 1|\_, v_j)$ with the outcomes of v_j being 0 and 1, respectively, for all v_i adjacent to v_j) must be, within the experimental error, compatible with zero, while this error should be equal to the one affecting the influence between second measurements and first measurements (denoted as $\varepsilon(0,\_\,|v_i,\_\,)$ and $\varepsilon(1,\_\,|v_i,\_\,)$ with the outcomes of v_i being 0 and 1, respectively, for all v_j adjacent to v_i) , which, according to causality, is zero. More precisely, $\varepsilon(\_, 0|\_, v_j) \approx \varepsilon(0,\_\,|v_i,\_\,) = 0$, $\varepsilon(\_, 1|\_, v_j) \approx \varepsilon(1,\_\,|v_i,\_\,) = 0$, where the definitions of $\varepsilon(\_, 0|\_, v_j)$, $\varepsilon(0,\_\,|v_i,\_\,)$, $\varepsilon(\_, 1|\_, v_j)$, and $\varepsilon(1,\_\,|v_i,\_\,)$ can be found in Appendix B.2.

Optics EXPRESS

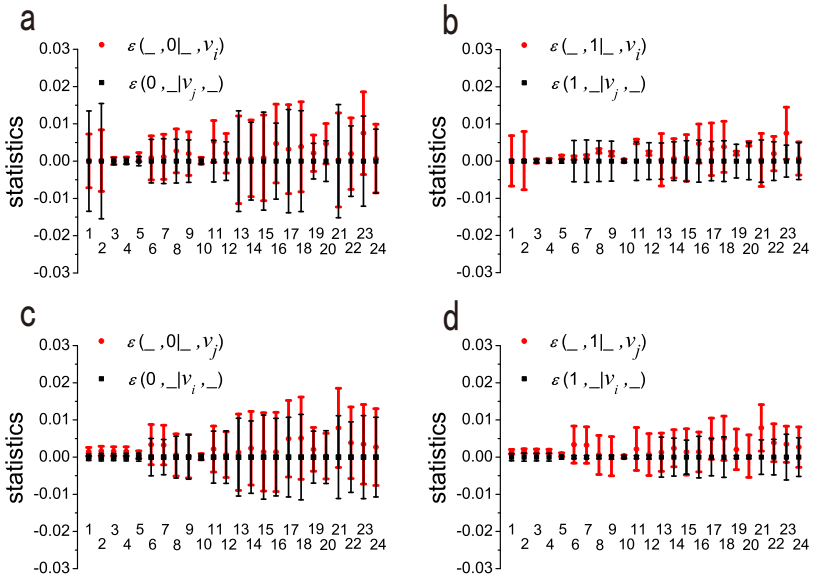

Fig. 3. Influence between adjacent measurements with the input state $|\varphi_1\rangle(=|i_1\rangle)$. The numbers along the x axis represent the settings of (v_i, v_j) as (v_1, v_2) (number 1), (v_1, v_3) (number 2), (v_1, v_4) (number 3), (v_1, v_7) (number 4), (v_2, v_3) (number 5), (v_2, v_5) (number 6), (v_2, v_8) (number 7), (v_3, v_6) (number 8), (v_3, v_9) (number 9), (v_4, v_7) (number 10), (v_4, v_{10}) (number 11), (v_4, v_{13}) (number 12), (v_5, v_{13}) (number 13), (v_5, v_8) (number 14), (v_5, v_{11}) (number 15), (v_6, v_9) (number 16), (v_6, v_{13}) (number 17), (v_6, v_{12}) (number 18), (v_7, v_{12}) (number 19), (v_7, v_{11}) (number 20), (v_8, v_{12}) (number 21), (v_8, v_{10}) (number 22), (v_9, v_{10}) (number 23), (v_9, v_{11}) (number 24). The error bars are estimated from counting statistics.

Figure 3 shows the experimental influence between measurements for the input sate $|\varphi_1\rangle(=|i_1\rangle)$. It clearly shows that, for that input state, our experiment satisfies the no-signaling condition. The errors are estimated from the counting statistics which are assumed to follow a Poisson distribution (see Appendix B.3 for more details). In Appendix B.4, we provide detailed results for other six input states, showing that no-signaling is also achieved in these cases.

The experimental results violating inequality (3) are shown in Fig. 4. We test the inequality with different pure and mixed states. We observe that the inequality (3) is violated, almost uniformly, for all the states tested in experiment and that the experimental values never surpass the quantum bound for sharp measurements.

4. Discussion

We have observed for the first time the optimal form of quantum state-independent contextuality respecting the condition of no-signaling between the measurements in the same context, which is essential to make sense of any test of contextuality. Our experimental results agree with the quantum predictions and confirm the existence of contextual correlations between sequential compatible measurements which are independent of the initial state of the system.

Different from the optimal inequality in terms of the dichotomic observables found by Kleinmann *et al.* [26], the proposed optimal inequality in the form of projective operators is more closer related to the graph theory. It is due to the fact that the carefully chosen amplitudes in the inequality reflects the fractional chromatic number and the symmetry of the exclusivity graph [27]. We further discuss the relations between these two forms in Appendix A.

Optics EXPRESS

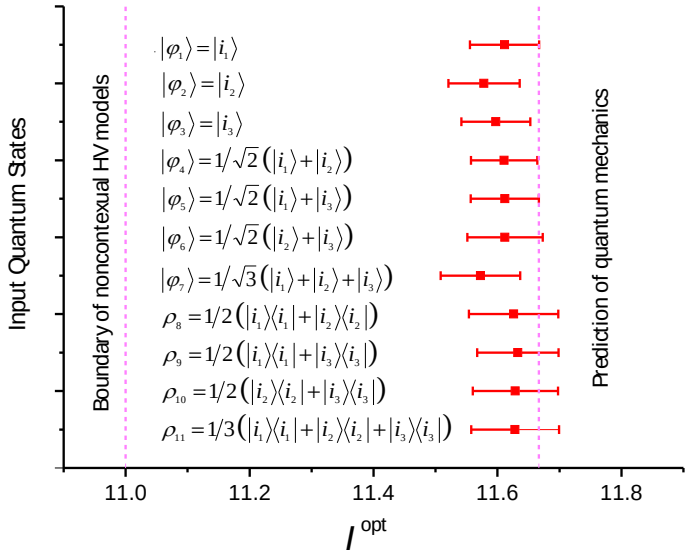

Fig. 4. The experimental results of I^{opt} (shown by the red squares) with different input states. For all states, we obtain a violation of the inequality, which demonstrates its state-independent character. The dashed line in the left-hand side specifies the upper bound imposed by noncontextual hidden variable (HV) models, while the dashed line in the right-hand side corresponds to the quantum mechanical prediction. The error bars are estimated from the counting statistics.

However, our experiment is not perfect in several senses. One is due to the intrinsic limitation that suppose using photons or any other quantum systems in which perfectly projective nondemolition measurements are difficult to achieve. This forces us to adopt the method proposed in [23], which consists of two stages: Stage one tests no-signaling. Once this test is satisfied, stage two tests the violation of the NCI. However, stage one requires a repreparation that depends on the initial state and only constitutes a simulation of a truly sequential projective measurement. Another limitation of our experiment is its imperfect detection efficiency, which forces us to make the assumption of fair sampling. The preferable way to solve these two problems is to use trapped ions for seqential projection measurements [28]. In this work, we directly measure the statistic between sequential measurements, in which the communication between them is not apparent at the level of statistics. It has been recently proposed to distinguish a truly quantum system that is measured sequentially from classical system by measuring heat [29–31]. We anticipate experimental progress in this direction in the near future.

Optics EXPRESS

Appendices

A. Proof of the optimality of inequality (2)

The Yu-Oh set consists of 13 observables $\hat{P}_i = |v_i\rangle\langle v_i|$. Explicitly, they are

$$\hat{P}_1 = \begin{bmatrix} 1 & 0 & 0 \\ 0 & 0 & 0 \\ 0 & 0 & 0 \end{bmatrix}, \quad \hat{P}_2 = \begin{bmatrix} 0 & 0 & 0 \\ 0 & 1 & 0 \\ 0 & 0 & 0 \end{bmatrix}, \quad \hat{P}_3 = \begin{bmatrix} 0 & 0 & 0 \\ 0 & 0 & 0 \\ 0 & 0 & 1 \end{bmatrix},$$
$$\hat{P}_4 = \frac{1}{2}\begin{bmatrix} 0 & 0 & 0 \\ 0 & 1 & -1 \\ 0 & -1 & 1 \end{bmatrix}, \quad \hat{P}_5 = \frac{1}{2}\begin{bmatrix} 1 & 0 & -1 \\ 0 & 0 & 0 \\ -1 & 0 & 1 \end{bmatrix},$$
$$\hat{P}_6 = \frac{1}{2}\begin{bmatrix} 1 & -1 & 0 \\ -1 & 1 & 0 \\ 0 & 0 & 0 \end{bmatrix}, \quad \hat{P}_7 = \frac{1}{2}\begin{bmatrix} 0 & 0 & 0 \\ 0 & 1 & 1 \\ 0 & 1 & 1 \end{bmatrix},$$
$$\hat{P}_8 = \frac{1}{2}\begin{bmatrix} 1 & 0 & 1 \\ 0 & 0 & 0 \\ 1 & 0 & 1 \end{bmatrix}, \quad \hat{P}_9 = \frac{1}{2}\begin{bmatrix} 1 & 1 & 0 \\ 1 & 1 & 0 \\ 0 & 0 & 0 \end{bmatrix},$$
$$\hat{P}_{10} = \frac{1}{3}\begin{bmatrix} 1 & -1 & -1 \\ -1 & 1 & 1 \\ -1 & 1 & 1 \end{bmatrix}, \quad \hat{P}_{11} = \frac{1}{3}\begin{bmatrix} 1 & -1 & 1 \\ -1 & 1 & -1 \\ 1 & -1 & 1 \end{bmatrix},$$
$$\hat{P}_{12} = \frac{1}{3}\begin{bmatrix} 1 & 1 & -1 \\ 1 & 1 & -1 \\ -1 & -1 & 1 \end{bmatrix}, \quad \hat{P}_{13} = \frac{1}{3}\begin{bmatrix} 1 & 1 & 1 \\ 1 & 1 & 1 \\ 1 & 1 & 1 \end{bmatrix}. \tag{5}$$

Let's say that $\vec{w} = \{w_1, w_2, \ldots, w_{13}\}$ is an optimal solution such that

$$I_{\mathrm{QM}}(\vec{w}) = \sum_{i=1}^{13} w_i \langle \hat{P}_i \rangle = w_0 \mathbb{1}. \tag{6}$$

Due to the fact that we consider the state-independent contextuality, w_0 is a constant and equals to $\sum_{i=1}^{13} w_i/3$.

There are 13 parameters (w_i) in Eq. (6) and it is difficult to determine the concrete optimal solution. We find that there are symmetric properties in $\hat{P}_i$, which can be used to reduce the number of parameters. Denote $F_{i,j}$ as the flip function which flips the sign of the elements at the positions (i, j) and (j, i). Under the operation of the combined flip function $F_{1,2}F_{1,3}$, in the left-hand side of Eq. (6), $\hat{P}_5$ is changed to $\hat{P}_8$ and $\hat{P}_8$ is changed to $\hat{P}_5$. We denote the case to be $(\hat{P}_5 \leftrightarrow \hat{P}_8)$. Similarly, $(\hat{P}_6 \leftrightarrow \hat{P}_9)$, $(\hat{P}_{10} \leftrightarrow \hat{P}_{13})$ and $(\hat{P}_{11} \leftrightarrow \hat{P}_{12})$ also hold under the operation of $F_{1,2}F_{1,3}$. The other terms of $\hat{P}_i$ remain the same under the operation. The value in the right-hand side of Eq. (6) remains unchanged. As a result, we can simplify the parameters and keep Eq. (6) remains optimal as $w_5 = w_8$, $w_6 = w_9$, $w_{10} = w_{13}$ and $w_{10} = w_{12}$.

We can further obtain $(\hat{P}_4 \leftrightarrow \hat{P}_7)$, $(\hat{P}_6 \leftrightarrow \hat{P}_9)$, $(\hat{P}_{11} \leftrightarrow \hat{P}_{13})$ and $(\hat{P}_{10} \leftrightarrow \hat{P}_{12})$ under the operation of $F_{1,2}F_{2,3}$; $(\hat{P}_4 \leftrightarrow \hat{P}_7)$, $(\hat{P}_5 \leftrightarrow \hat{P}_8)$, $(\hat{P}_{12} \leftrightarrow \hat{P}_{13})$ and $(\hat{P}_{10} \leftrightarrow \hat{P}_{11})$ under the operation of $(F_{1,2}F_{1,3})(F_{1,2}F_{2,3})$. The parameters are then simplified as $w_4 = w_7$, $w_{11} = w_{13}$, $w_{10} = w_{12}$, and $w_{12} = w_{13}$.

We further defined $S_{i,j}$ as the function which exchanges the i-th rows and j-th rows, and then exchange the i-th column and j-th column of $\hat{P}_i$. We then obtain $(\hat{P}_1 \leftrightarrow \hat{P}_2)$, $(\hat{P}_4 \leftrightarrow \hat{P}_5)$, $(\hat{P}_7 \leftrightarrow \hat{P}_8)$ and $(\hat{P}_{10} \leftrightarrow \hat{P}_{11})$ under the operation of $S_{1,2}$; $(\hat{P}_1 \leftrightarrow \hat{P}_3)$, $(\hat{P}_4 \leftrightarrow \hat{P}_6)$, $(\hat{P}_7 \leftrightarrow \hat{P}_9)$ and $(\hat{P}_{10} \leftrightarrow \hat{P}_{12})$ under the operation of $S_{1,3}$; $(\hat{P}_2 \leftrightarrow \hat{P}_3)$, $(\hat{P}_5 \leftrightarrow \hat{P}_6)$, $(\hat{P}_8 \leftrightarrow \hat{P}_9)$ and $(\hat{P}_{11} \leftrightarrow \hat{P}_{12})$ under the operation of $S_{1,3}S_{1,2}S_{1,3}$. Similarly, except the exchanged terms, the other $\hat{P}_i$ and the

value in the right-hand side of Eq. (6) remains unchanged under the corresponding operation of $S_{i,j}$. As a result, we further simplify the parameters to be $w_1 = w_2$, $w_4 = w_5$, $w_7 = w_8$, $w_1 = w_3$, $w_4 = w_6$, $w_7 = w_9$ and $w_5 = w_6$.

Finally, the simplified new optimal parameters become

$$w_1 = w_2 = w_3, w_4 = w_5 = w_6 = w_7 = w_8 = w_9, w_{10} = w_{11} = w_{12} = w_{13}. \tag{7}$$

That is, $I_{\rm QM} = w_1 + 2w_4 + 4w_{10}/3$ in the quantum case, while the noncontextual hidden variable bound is the weighted independence $\alpha(\vec{w})$ where

$$\alpha(\vec{w}) \quad = \quad \max\{w_1 + 4w_{10}, w_1 + w_{10} + 2w_4, w_{10} + 3w_4\}. \tag{8}$$

Let's assume $w_{10} = 1$ for convenience, then $I_{\rm QM} = w_1 + 2w_4 + 4/3$ and

$$\alpha = \max\{w_1 + 4, w_1 + 2w_4 + 1, 1 + 3w_4\}. \tag{9}$$

If $\alpha = w_1 + 4$, then $w_4 \leq \min\{3/2, 1 + w_1/3\}$,

$$r = \frac{I_{\rm QM}}{\alpha} = \frac{w_1 + 2w_4 + 4/3}{w_1 + 4} = \begin{cases} (w_1 + 13/3)/(w_1 + 4), & w_1 \geq 3/2, \\ (5w_1/3 + 10/3)/(w_1 + 4), & w_1 \leq 3/2. \end{cases} \tag{10}$$

Thus the optimal value is $r = 35/33$ when $w_1 = w_4 = 3/2$. In the similar analysis of the rest two cases, we'll get the same solution.

Based on the above analysis, one finds that for $w_1/w_{10} = w_4/w_{10} = 3/2$, the ratio $r = I_{\rm QM}/\alpha = 35/33 \approx 1.0606$ is maximal, thus the optimal NC inequality becomes

$$I = 3\sum_{i=1}^{9}\langle\hat{P}_i\rangle + 2\sum_{i=10}^{13}\langle\hat{P}_i\rangle \leq 11, \tag{11}$$

which is the inequality (2) in the main text. This ends the proof.

Remark 1.—In [12], Yu and Oh have presented the first SIC inequality for the Yu-Oh set (see the inequality (4) in [12]). The SIC inequality is written in terms of the dichotomic observables $\hat{A}$. According to the relation $\hat{A}_i = \mathbb{1} - 2\hat{P}_i$ between these observables, the Yu-Oh SIC inequality can be recast to the SIC inequality in terms of observables as

$$I = 2\sum_{i=1}^{9}\langle\hat{P}_i\rangle + \sum_{i=10}^{13}\langle\hat{P}_i\rangle \leq 7, \tag{12}$$

i.e., $w_1/w_{10} = 2$ and $\alpha = 7$. The quantum violation is $I_{\rm QM} = 22/3$, thus the ratio $r = I_{\rm QM}/\alpha = 22/21 \approx 1.0476 \leq 35/33$.

Remark 2.—In [26], Kleinmann *et al.* have investigated the optimal SIC inequalities in terms of the dichotomic observables $\hat{A}$ (see Table I in [26]). They have found the optimal tight NC inequalities for contexts of maximal size two (called "$\rm opt_2$") and size three (called "$\rm opt_3$"), respectively. Similarly, for the NC inequality "$\rm opt_2$", one can recast it to the SIC inequality in terms of observables as

$$I = 3\sum_{i=1,4,7,10,11,12,13}\langle\hat{P}_i\rangle + 6\sum_{i=2,3,5,6,8,9}\langle\hat{P}_i\rangle \leq 18, \tag{13}$$

whose symmetrical version is

$$I = 5\sum_{i=1}^{9}\langle\hat{P}_i\rangle + 3\sum_{i=10}^{13}\langle\hat{P}_i\rangle \leq 18, \tag{14}$$

Optics EXPRESS

i.e., $w_1/w_{10} = 5/3$ and $\alpha = 18$. The quantum violation is $I_{\rm QM} = 19$, thus the ratio $r = I_{\rm QM}/\alpha = 19/18 \approx 1.0555 \leq 35/33$. Interestingly, by adding inequalities (11) and (12), one may have the inequality (14).

Remark 3.—Because the ratio $r = \frac{35}{33}$ is the largest, the SIC inequality (11) will be more friendly to the experiment. To test the quantum SIC under the no-signaling condition, based on the method in [23] we need to transform the NC inequality (11) to the following form

$$\begin{aligned} I^{\rm opt} = & 3\sum_{i=1}^{9} P_{|\varphi\rangle}(v_i = 1)\left(1 - \frac{1}{2}\sum_{(i,j)\in E} P_{|v_i\rangle}(v_j = 1)\right) \\ & + 2\sum_{i=10}^{13} P_{|\varphi\rangle}(v_i = 1)\left(1 - \frac{1}{2}\sum_{(i,j)\in E} P_{|v_i\rangle}(v_j = 1)\right) \\ & \leq 11, \end{aligned} \tag{15}$$

by replacing each projector $\langle \hat{P}_i \rangle \equiv P_{|\varphi\rangle}(v_i = 1)$ with

$$P_{|\varphi\rangle}(v_i = 1) - \frac{1}{2}\sum_{(i,j)\in E} P_{|\varphi\rangle}(v_i = 1, v_j = 1). \tag{16}$$

Here $|\varphi\rangle$ is the initial quantum state, and the edge set E with $(i, j) \in E$ indicates that $|v_i\rangle$ and $|v_j\rangle$ are orthogonal, i.e., $\langle v_i|v_j\rangle = 0$. Remarkably, the resultant NC inequality (15) keeps the same classical bound and quantum violation as the inequality (2) [23]. The two-point probability $P_{|\varphi\rangle}(v_i = 1, v_j = 1)$ will be calculated through

$$P_{|\varphi\rangle}(v_i = 1, v_j = 1) = P_{|\varphi\rangle}(v_i = 1)P_{|v_i\rangle}(v_j = 1), \tag{17}$$

which represents the successive measurements. All non-contextual hidden variables models satisfy the inequality (15), while the quantum theory predicts that, for any qutrit state, $I_{\rm QM} = 35/3$. Thus the inequality (15) can be used to test quantum SIC of a qutrit under the no-signaling condition, which is checked in detail in the experimental part.

B. Experimental details

B.1. The preparation of a single photon source

A 632.8 nm laser is used to excite the 4H-SiC sample, as shown in Fig. 2 in the main text. After being reflected by a dichroic mirror, the laser is focused onto the sample by an objective lens with a high-NA (0.95). The sample used was diced from a 350-um-thick wafer of high-purity semi-insulating 4H-SiC purchased from CREE (part number: W4TRE0R-0200), and had dimensions of roughly 5 mm × 10 mm. To increase the defects in the samples, they were irradiated with 10 MeV electrons. After the irradiation, anneals at 800° C in an Ar ambient for 30 min were carried out. The fluorescence is then filtered by the dichroic mirror and a bandpass filter with a center wavelength at 720 nm and a bandwidth of 13 nm. The fluorescence light is sent to a fiber beam-splitter and then coupled onto two single photon avalanche photodiodes (SPADs) to record the detection time difference τ. The breakdown emissions from the SPADs was delayed by increasing the length of fibers to 5 m. The autocorrelation of the emission, showed in Fig. 5, show a clear signature of photon antibunching around $\tau = 0$ with the experimental value of $g^2(0) = 0.179$ and a theoretical fitting of $g^2(0) = 0.026$. It demonstrates that the source is a genuine single photon source. After the autocorrelation function is measured, the photon is sent to the contextuality setup for further verification.

Optics EXPRESS

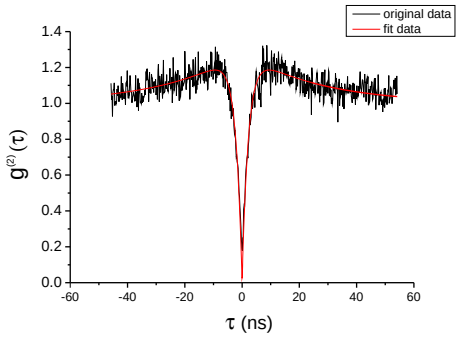

Fig. 5. The second-order photon correlation function ($g^2(\tau)$) as a function of the delay time τ. $g^2(0) = 0.179$ with a fitting to 0.026 clearly confirms the character of single-photon emission.

B.2. The method to measure $P_{|\varphi\rangle}(v_i = 0, v_j = 1)$

In any test of contextuality, we should achieve no-signaling between the measurements in the same context. According to [23], the influence of the first measurements on the second measurements for all v_i adjacent to v_j can be calculated as:

$$\varepsilon(\_,0|\_,v_j) = |P_{|\varphi\rangle}(v_j = 0) - P_{|\varphi\rangle}(v_i = 0, v_j = 0) - P_{|\varphi\rangle}(v_i = 1, v_j = 0)|, \tag{18}$$

$$\varepsilon(\_,1|\_,v_j) = |P_{|\varphi\rangle}(v_j = 1) - P_{|\varphi\rangle}(v_i = 0, v_j = 1) - P_{|\varphi\rangle}(v_i = 1, v_j = 1)|, \tag{19}$$

where $\varepsilon(\_,0|\_,v_j)$ and $\varepsilon(\_,1|\_,v_j)$ represent the cases when the outcomes of v_j are 0 and 1, respectively. The influence of the second measurements on the first measurements for all v_j adjacent to v_i can be calculated as:

$$\varepsilon(0,\_\,|v_i,\_\,) = |P_{|\varphi\rangle}(v_i = 0) - P_{|\varphi\rangle}(v_i = 0, v_j = 0) - P_{|\varphi\rangle}(v_i = 0, v_j = 1)|, \tag{20}$$

$$\varepsilon(1,\_\,|v_i,\_\,) = |P_{|\varphi\rangle}(v_i = 1) - P_{|\varphi\rangle}(v_i = 1, v_j = 0) - P_{|\varphi\rangle}(v_i = 1, v_j = 1)|, \tag{21}$$

where $\varepsilon(0,\_\,|v_i,\_\,)$ and $\varepsilon(1,\_\,|v_i,\_\,)$ represent the cases when the outcomes of v_i are 0 and 1, respectively.

The corresponding probabilities are calculated as

$$\begin{aligned}
P_{|\varphi\rangle}(v_i = 0) &= 1 - P_{|\varphi\rangle}(v_i = 1),\\
P_{|\varphi\rangle}(v_i = 1, v_j = 1) &= P_{|\varphi\rangle}(v_i = 1)P_{|v_i\rangle}(v_j = 1),\\
P_{|\varphi\rangle}(v_i = 0, v_j = 1) &= P_{|\varphi\rangle}(v_i = 0)P_{|v_i^{\perp}\rangle}(v_j = 1),\\
P_{|\varphi\rangle}(v_i = 1, v_j = 0) &= P_{|\varphi\rangle}(v_i = 1) - P_{|\varphi\rangle}(v_i = 1, v_j = 1),\\
P_{|\varphi\rangle}(v_i = 0, v_j = 0) &= P_{|\varphi\rangle}(v_i = 0) - P_{|\varphi\rangle}(v_i = 0, v_j = 1).
\end{aligned} \tag{22}$$

In the experiment, We need to check that

$$\begin{aligned}
\varepsilon(_,0|_,v_j) &\approx \varepsilon(0,_\,|v_i,_\,) = 0,\\
\varepsilon(_,1|_,v_j) &\approx \varepsilon(1,_\,|v_i,_\,) = 0.
\end{aligned} \tag{23}$$

In order to obtain $P_{|\varphi\rangle}(v_i = 0, v_j = 1)$, we need to prepare $|v_i^{\perp}\rangle$, which is the state obtained after a projective measurement of v_i with outcome 0 on a system initially prepared in state $|\varphi\rangle$.

Optics EXPRESS

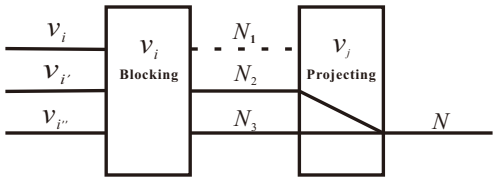

Fig. 6. The setup to detect $P_{|\varphi\rangle}(v_i = 0, v_j = 1)$

This is realized by the blocking method. The setup to detect $P_{|\varphi\rangle}(v_i = 0, v_j = 1)$ is shown in Fig. 6 and the detailed process is shown below.

(1). We express the input state $|\varphi\rangle$ in the complete basis of $\{v_i, v_{i'}, v_{i''}\}$. The normalized state can be written as $|\varphi\rangle = \alpha|v_i\rangle + \beta|v_{i'}\rangle + \gamma|v_{i''}\rangle$, where $|\alpha|^2 + |\beta|^2 + |\gamma|^2 = 1$. We denote the counting rate in each basis to be N_1, N_2 and N_3, respectively. We obtain $P_{|\varphi\rangle}(v_i = 0) = \dfrac{N_2 + N_3}{N_1 + N_2 + N_3}$.

(2). The part of v_i is blocked, and the remain state ($|v_i^{\perp}\rangle$) is further projected to the vector of $|v_j\rangle$ with the counting rate denoted as N. We obtain $P_{|v_i^{\perp}\rangle}(v_j = 1) = \dfrac{N}{N_2 + N_3}$.

(3). $P_{|\varphi\rangle}(v_i = 0, v_j = 1) = \dfrac{N}{N_1 + N_2 + N_3}$.

B.3. Error estimation

In our experiment, the statistics of each count (N) is assumed to follow a Poisson distribution. We use a subprogram of Poisson Distribution in Wolfram Mathematica 9.0 to simulate the Poisson distribution. The values of each measurement quantity are then calculated from 50 randomly grouped counting sets, in which the error of the quantity is estimated by the standard deviation (SD). To obtain the error of the final value we want (I^{opt} and ε), we sum all the errors of the measured quantities included in the calculation. For example, the error of I^{opt} is calculated as

$$\begin{aligned} SD(I^{\text{opt}}) = 3\sum_{i=1}^{9} SD(P_{|\varphi\rangle}(v_i = 1)(1 + \frac{1}{2}\sum_{(i,j)\in E} P_{|v_i\rangle}(v_j = 1))) \\ + 2\sum_{i=10}^{13} SD(P_{|\varphi\rangle}(v_i = 1)(1 + \frac{1}{2}\sum_{(i,j)\in E} P_{|v_i\rangle}(v_j = 1))). \end{aligned} \tag{24}$$

In our experiment, the maximal error for ε to obtain the no-signaling condition is about 0.02 and we observe a clear violation of inequality (3) which is shown in Fig. 4.

B.4. More experimental results

The experimental results of the measurement statistical effect for input states from $|\varphi_2\rangle$ to $|\varphi_7\rangle$ are showed in Figs. 7–12 (the one for the input state $|\varphi_1\rangle$ is shown in Fig. 3 in the main text). The results clearly imply that our experiment satisfied the no-signaling conditions.

Optics EXPRESS

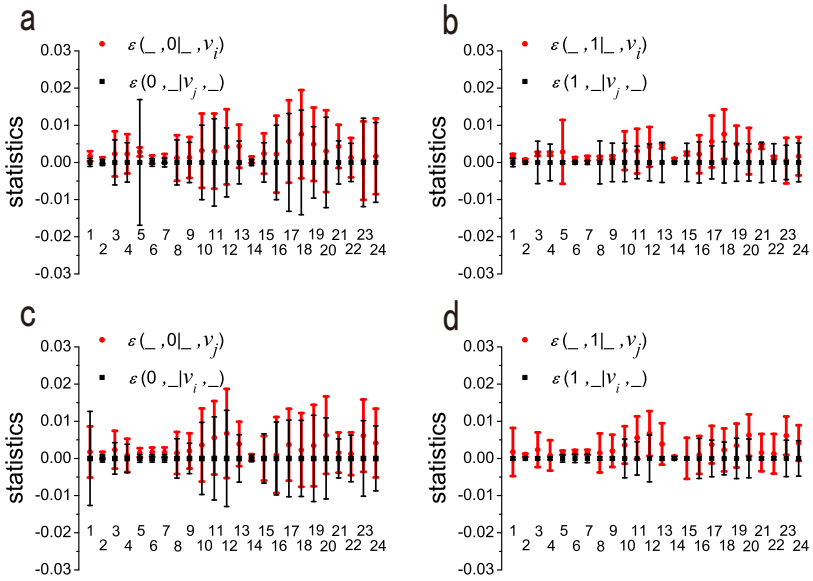

Fig. 7. Influence between adjacent measurements with the input state $|\varphi_2\rangle$ (= $|i_2\rangle$). The numbers along the x axis represent the settings of (v_i, v_j) as (v_1, v_2) (number 1), (v_1, v_3) (number 2), (v_1, v_4) (number 3), (v_1, v_7) (number 4), (v_2, v_3) (number 5), (v_2, v_5) (number 6), (v_2, v_8) (number 7), (v_3, v_6) (number 8), (v_3, v_9) (number 9), (v_4, v_7) (number 10), (v_4, v_{10}) (number 11), (v_4, v_{13}) (number 12), (v_5, v_{13}) (number 13), (v_5, v_8) (number 14), (v_5, v_{11}) (number 15), (v_6, v_9) (number 16), (v_6, v_{13}) (number 17), (v_6, v_{12}) (number 18), (v_7, v_{12}) (number 19), (v_7, v_{11}) (number 20), (v_8, v_{12}) (number 21), (v_8, v_{10}) (number 22), (v_9, v_{10}) (number 23), (v_9, v_{11}) (number 24). The error bars are estimated from counting statistics.

Optics EXPRESS

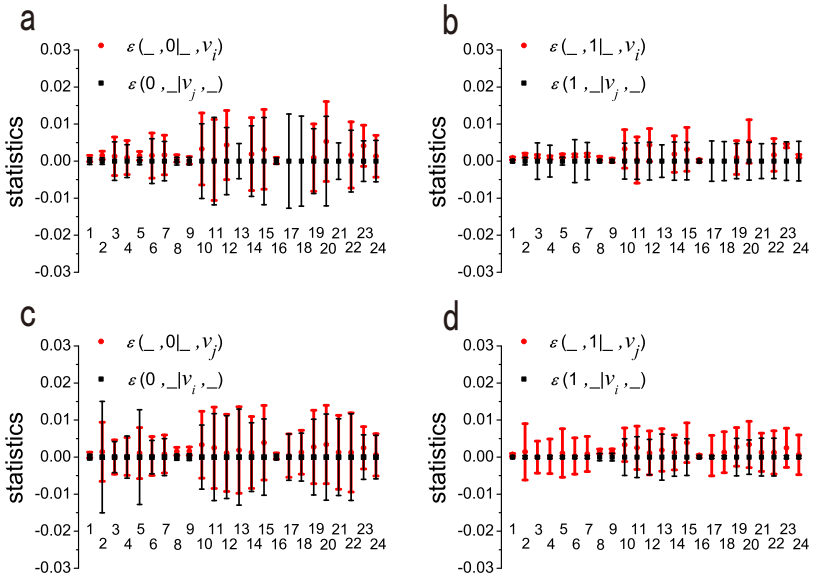

Fig. 8. Influence between adjacent measurements with the input state $|\varphi_3\rangle$ (= $|i_3\rangle$). The numbers along the x axis represent the settings of (v_i, v_j) as (v_1, v_2) (number 1), (v_1, v_3) (number 2), (v_1, v_4) (number 3), (v_1, v_7) (number 4), (v_2, v_3) (number 5), (v_2, v_5) (number 6), (v_2, v_8) (number 7), (v_3, v_6) (number 8), (v_3, v_9) (number 9), (v_4, v_7) (number 10), (v_4, v_{10}) (number 11), (v_4, v_{13}) (number 12), (v_5, v_{13}) (number 13), (v_5, v_8) (number 14), (v_5, v_{11}) (number 15), (v_6, v_9) (number 16), (v_6, v_{13}) (number 17), (v_6, v_{12}) (number 18), (v_7, v_{12}) (number 19), (v_7, v_{11}) (number 20), (v_8, v_{12}) (number 21), (v_8, v_{10}) (number 22), (v_9, v_{10}) (number 23), (v_9, v_{11}) (number 24). The error bars are estimated from counting statistics.

Optics EXPRESS

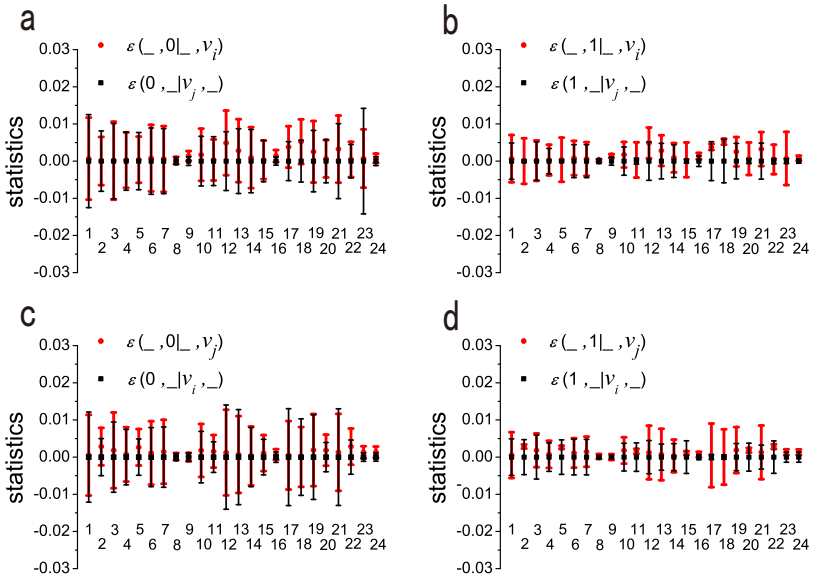

Fig. 9. Influence between adjacent measurements with the input state $|\varphi_4\rangle$ $(= \frac{1}{\sqrt{2}}(|i_1\rangle + |i_2\rangle))$. The numbers along the x axis represent the settings of (v_i, v_j) as (v_1, v_2) (number 1), (v_1, v_3) (number 2), (v_1, v_4) (number 3), (v_1, v_7) (number 4), (v_2, v_3) (number 5), (v_2, v_5) (number 6), (v_2, v_8) (number 7), (v_3, v_6) (number 8), (v_3, v_9) (number 9), (v_4, v_7) (number 10), (v_4, v_{10}) (number 11), (v_4, v_{13}) (number 12), (v_5, v_{13}) (number 13), (v_5, v_8) (number 14), (v_5, v_{11}) (number 15), (v_6, v_9) (number 16), (v_6, v_{13}) (number 17), (v_6, v_{12}) (number 18), (v_7, v_{12}) (number 19), (v_7, v_{11}) (number 20), (v_8, v_{12}) (number 21), (v_8, v_{10}) (number 22), (v_9, v_{10}) (number 23), (v_9, v_{11}) (number 24). The error bars are estimated from counting statistics.

Optics EXPRESS

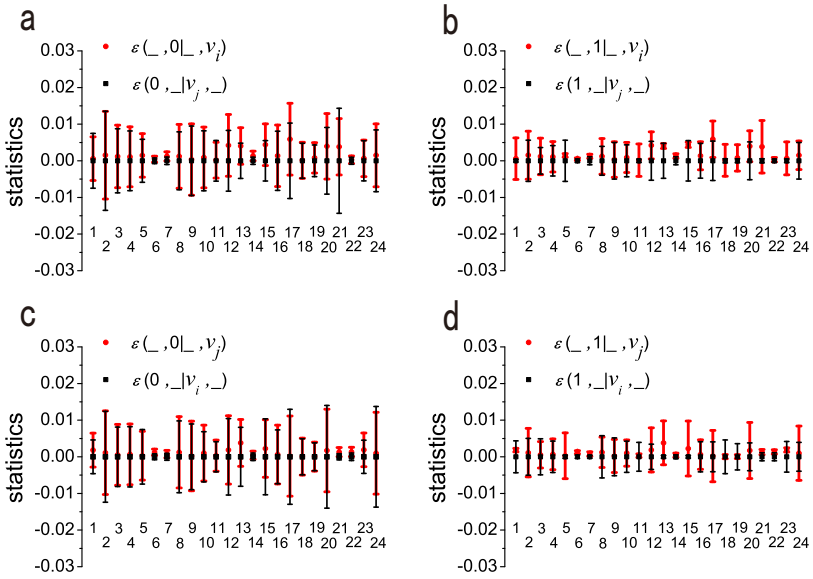

Fig. 10. Influence between adjacent measurements with the input state $|\varphi_5\rangle$ $(= \frac{1}{\sqrt{2}}(|i_1\rangle + |i_3\rangle))$. The numbers along the x axis represent the settings of (v_i, v_j) as (v_1, v_2) (number 1), (v_1, v_3) (number 2), (v_1, v_4) (number 3), (v_1, v_7) (number 4), (v_2, v_3) (number 5), (v_2, v_5) (number 6), (v_2, v_8) (number 7), (v_3, v_6) (number 8), (v_3, v_9) (number 9), (v_4, v_7) (number 10), (v_4, v_{10}) (number 11), (v_4, v_{13}) (number 12), (v_5, v_{13}) (number 13), (v_5, v_8) (number 14), (v_5, v_{11}) (number 15), (v_6, v_9) (number 16), (v_6, v_{13}) (number 17), (v_6, v_{12}) (number 18), (v_7, v_{12}) (number 19), (v_7, v_{11}) (number 20), (v_8, v_{12}) (number 21), (v_8, v_{10}) (number 22), (v_9, v_{10}) (number 23), (v_9, v_{11}) (number 24). The error bars are estimated from counting statistics.

Optics EXPRESS

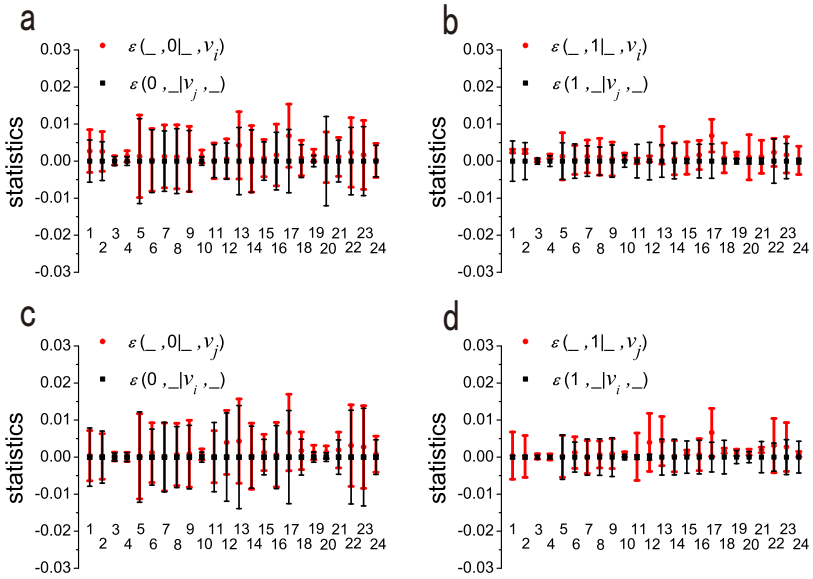

Fig. 11. Influence between adjacent measurements with the input state $|\varphi_6\rangle$ $(= \frac{1}{\sqrt{2}}(|i_2\rangle + |i_3\rangle))$. The numbers along the x axis represent the settings of (v_i, v_j) as (v_1, v_2) (number 1), (v_1, v_3) (number 2), (v_1, v_4) (number 3), (v_1, v_7) (number 4), (v_2, v_3) (number 5), (v_2, v_5) (number 6), (v_2, v_8) (number 7), (v_3, v_6) (number 8), (v_3, v_9) (number 9), (v_4, v_7) (number 10), (v_4, v_{10}) (number 11), (v_4, v_{13}) (number 12), (v_5, v_{13}) (number 13), (v_5, v_8) (number 14), (v_5, v_{11}) (number 15), (v_6, v_9) (number 16), (v_6, v_{13}) (number 17), (v_6, v_{12}) (number 18), (v_7, v_{12}) (number 19), (v_7, v_{11}) (number 20), (v_8, v_{12}) (number 21), (v_8, v_{10}) (number 22), (v_9, v_{10}) (number 23), (v_9, v_{11}) (number 24). The error bars are estimated from counting statistics.

Optics EXPRESS

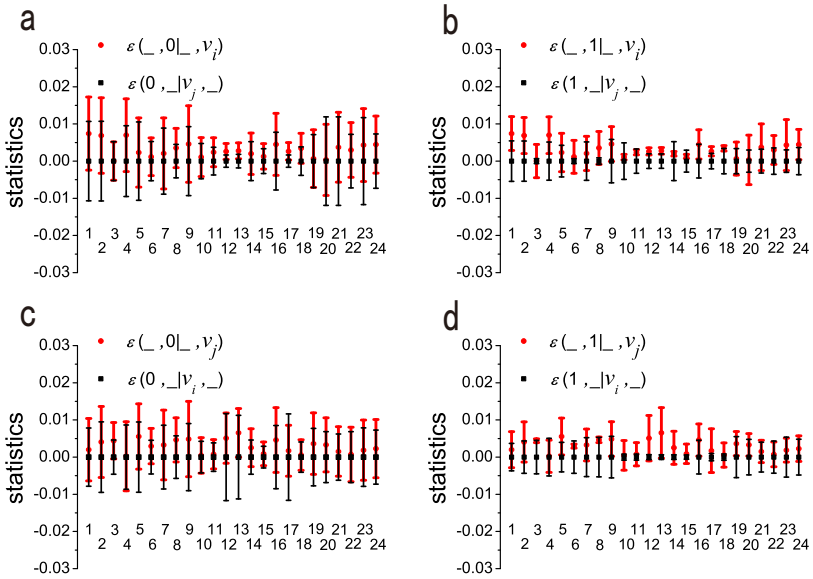

Fig. 12. Influence between adjacent measurements with the input state $|\varphi_7\rangle$ $(= \frac{1}{\sqrt{3}}(|i_1\rangle + |i_2\rangle + |i_3\rangle))$. The numbers along the x axis represent the settings of (v_i, v_j) as (v_1, v_2) (number 1), (v_1, v_3) (number 2), (v_1, v_4) (number 3), (v_1, v_7) (number 4), (v_2, v_3) (number 5), (v_2, v_5) (number 6), (v_2, v_8) (number 7), (v_3, v_6) (number 8), (v_3, v_9) (number 9), (v_4, v_7) (number 10), (v_4, v_{10}) (number 11), (v_4, v_{13}) (number 12), (v_5, v_{13}) (number 13), (v_5, v_8) (number 14), (v_5, v_{11}) (number 15), (v_6, v_9) (number 16),(v_6, v_{13}) (number 17), (v_6, v_{12}) (number 18), (v_7, v_{12}) (number 19), (v_7, v_{11}) (number 20), (v_8, v_{12}) (number 21), (v_8, v_{10}) (number 22), (v_9, v_{10}) (number 23), (v_9, v_{11}) (number 24). The error bars are estimated from counting statistics.

Funding

National Key Research and Development Program of China (2016YFA0302700 and 2017YFA0304100); National Natural Science Foundation of China (61327901, 61725504, 11325419, 61322506, 11475089, and 11774335); Strategic Priority Research Program (B) of CAS (XDB01030300); Key Research Program of Frontier Sciences, CAS (QYZDY-SSW-SLH003); Fundamental Research Funds for the Central Universities (WK2470000020 and WK2470000026); Youth Innovation Promotion Association and Excellent Young Scientist Program CAS; MISP (R0190-16-2028); Knut and Alice Wallenberg Foundation; MINECO.

Acknowledgments

H.Y.S. was supported by Institute for Information and Communications Technology Promotion (IITP) grant funded by the Korea Government (MSIP) (No. R0190-16-2028, "Practical and Secure Quantum Key Distribution"). J.L.C. was supported by the National Natural Science Foundation of China (Grants No. 11475089). A.C. was supported by Project No. FIS2014-60843-P, "Advanced Quantum Information" (MINECO, Spain), with FEDER funds and the project "Photonic Quantum Information" (Knut and Alice Wallenberg Foundation, Sweden).